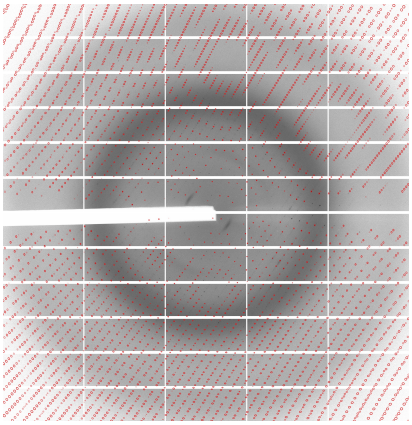
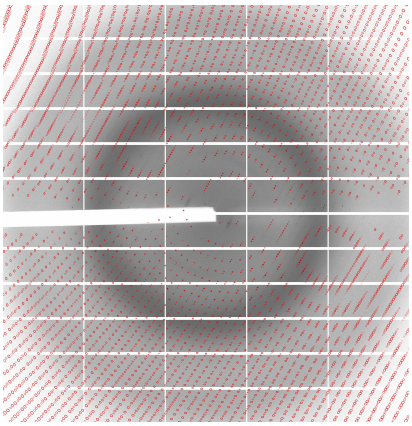
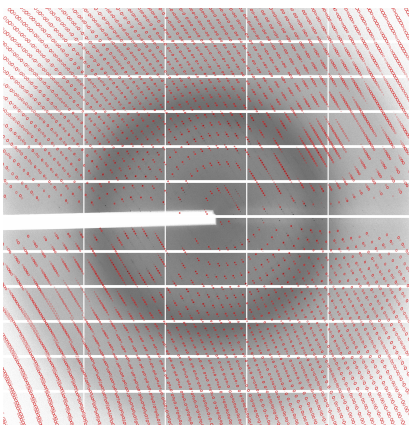
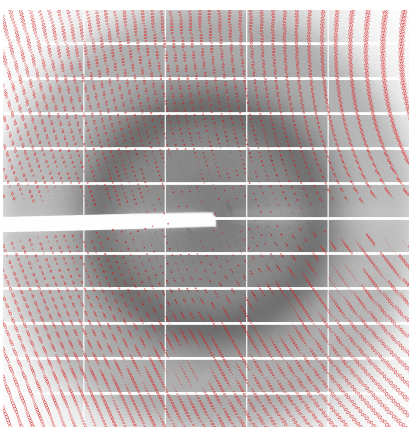

autoPROC	1.3.0 (20200318)
XDS	VERSION Jan 31, 2020 BUILT=20200131
AIMLESS	Version 0.7.4
STARANISO	Version 2.3.33 (11-Apr-2020)
CCP4	Version 7.0.078
Host	server8
User	vonrhein (group = users)
Date	Mon Apr 20 10:01:13 CEST 2020
autoPROC	/home/software/xtal/GPhL/20200420
m4G4eg	m4G4eg_#####.cbf (54 images, 27°)
m4G4eg-2	m4G4eg-2_#####.cbf (237 images, 118.5°)
m4G4eg-3	m4G4eg-3_#####.cbf (175 images, 87.5°)
m4G4eg-4	m4G4eg-4_#####.cbf (107 images, 53.5°)
m4G4eg-5	m4G4eg-5_#####.cbf (66 images, 33°)

Isotropic data analysis:

Spacegroup	P3121
Cell parameters	168.5282 168.5282 51.9549 90.0 90.0 120.0
Wavelength [A]	0.97918

	Overall	Inner Shell	Outer Shell
Low resolution limit	48.946	48.946	2.173
High resolution limit	2.136	5.796	2.136
Rmerge (all I+ & I-)	0.107	0.062	0.937
Rmeas (all I+ & I-)	0.111	0.064	1.003
Rpim (all I+ & I-)	0.027	0.016	0.354
Total number of observations	708930	41377	18327
Total number unique	47069	2462	2348
Mean(I)/sd(I)	20.1	49.9	2.4
Completeness	100.0	100.0	100.0
Multiplicity	15.1	16.8	7.8
CC(1/2)	0.999	0.999	0.774
Anomalous completeness	99.9	100.0	99.6
Anomalous multiplicity	7.7	9.0	4.0
CC(ano)	-0.148	-0.177	-0.001
|DANO|/sd(DANO)	0.792	1.084	0.728

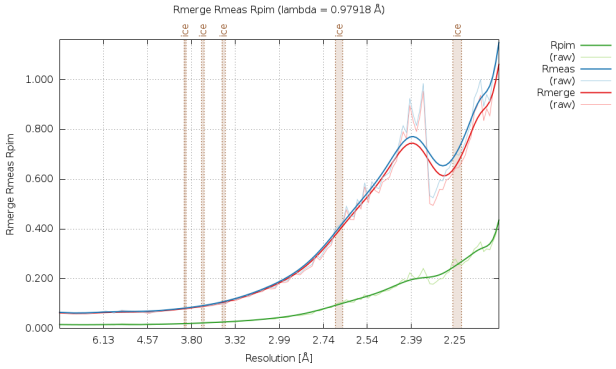

Fig.1 : R-values as a function of resolution

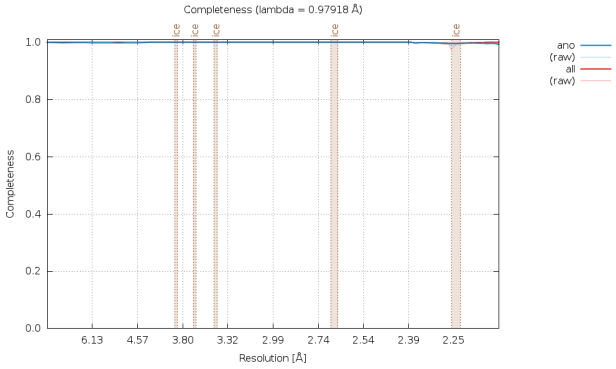

Fig.2 : Completeness as a function of resolution

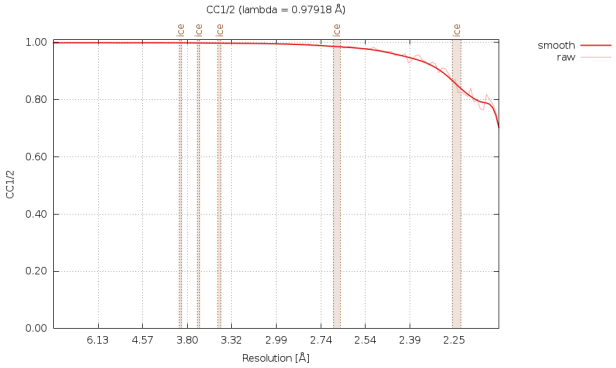

Fig.3 : CC1/2 as a function of resolution

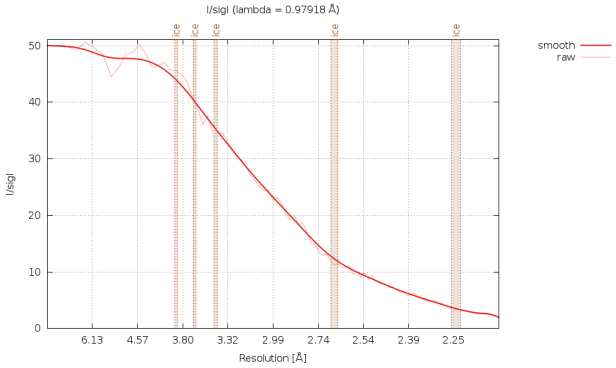

Fig.4 : I/sigI as a function of resolution

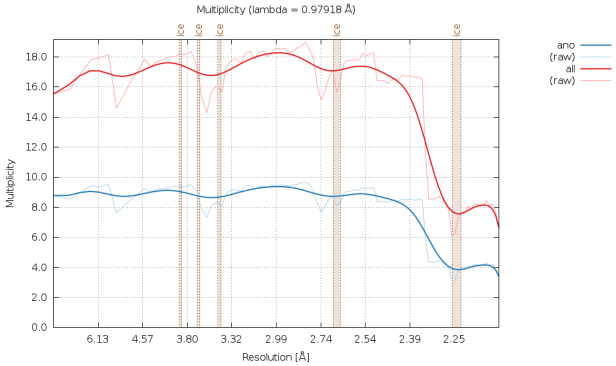

Fig.5 : Multiplicity as a function of resolution

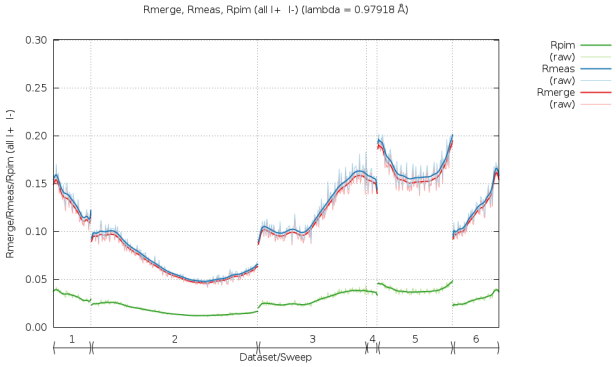

Fig.6 : R-values as a function of image number

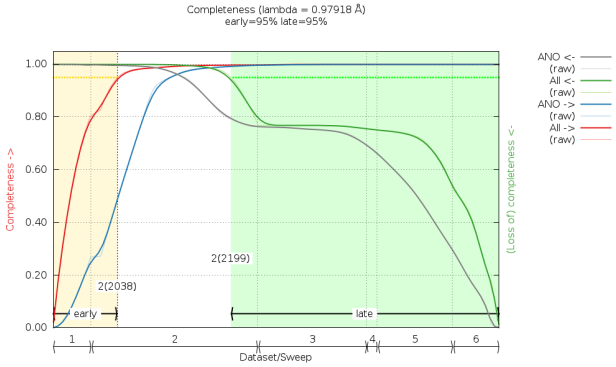

Fig.7 : Completeness as a function of image number

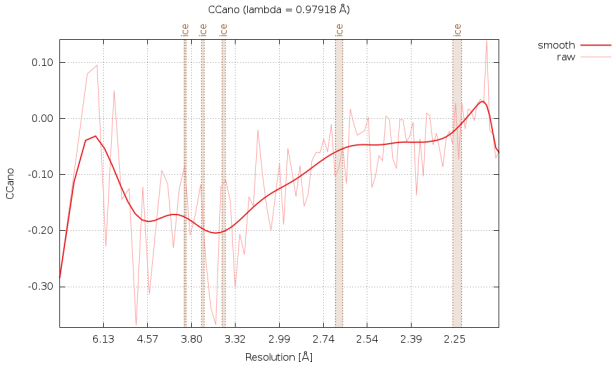

Fig.8 : CCano as a function of resolution

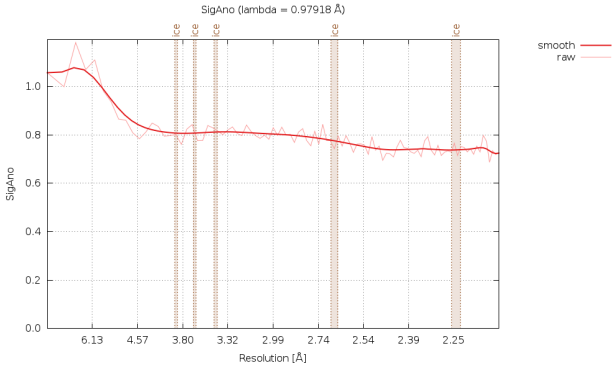

Fig.9 : SigAno as a function of resolution

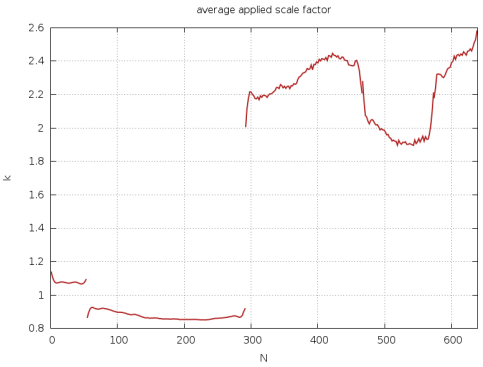

Fig.10 : Scale factor (AIMLESS scaling) as a function of image number

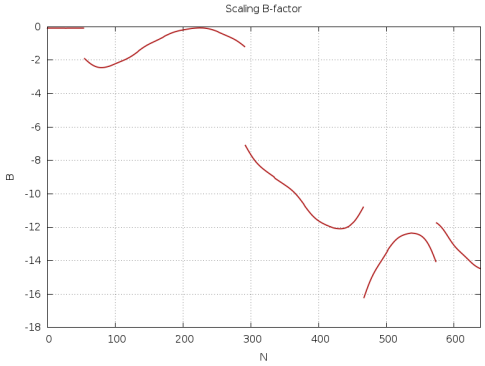

Fig.11 : Scaling B-factor (AIMLESS scaling) as a function of image number

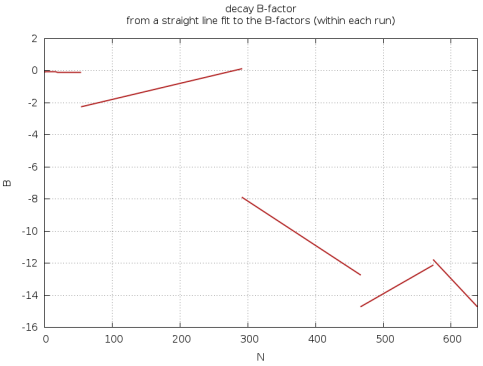

Fig.12 : Decay B-factor (AIMLESS scaling) as a function of image number

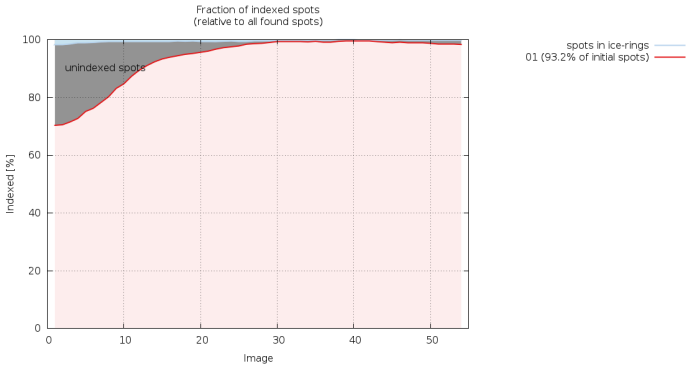

Fig.13 : (sweep m4G4eg) number of spots for each indexing solution as a function of image number

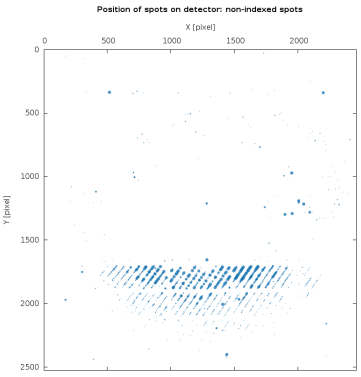

Fig.14 : (sweep m4G4eg) unindexed spots as a function of detector position

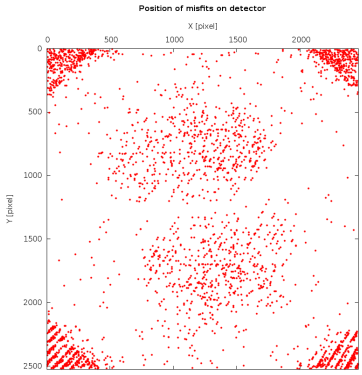

Fig.15 : (sweep m4G4eg) reflections classified as misfits (as a function of detector position)

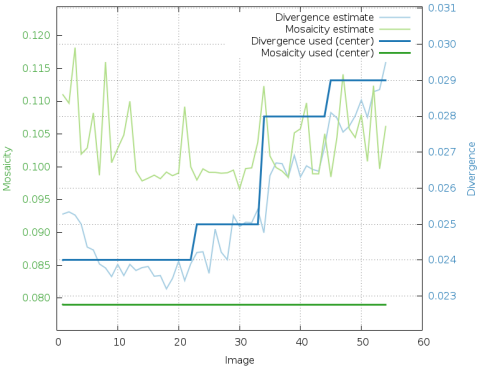

Fig.16 : (sweep m4G4eg) divergence and mosaicity (estimated and used) as a function of image number

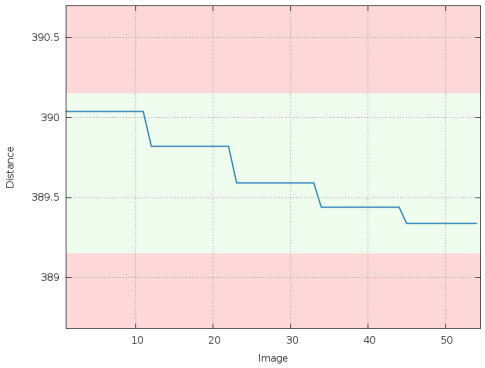

Fig.17 : (sweep m4G4eg) refined crystal-to-detector distance as a function of image number

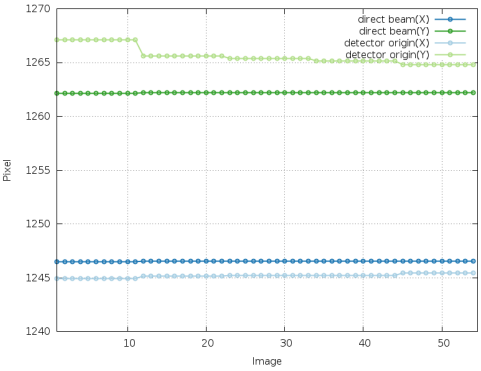

Fig.18 : (sweep m4G4eg) direct beam position and detector origin as a function of image number

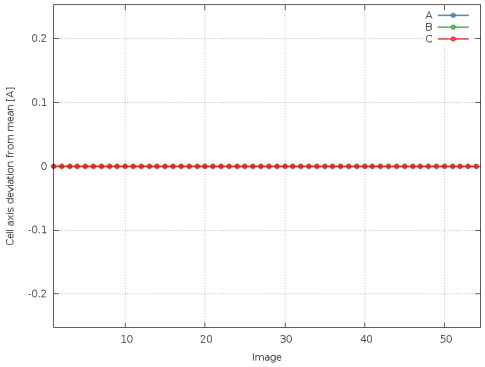

Fig.19 : (sweep m4G4eg) deviation of refined cell axes relative to their mean (as a function of image number)

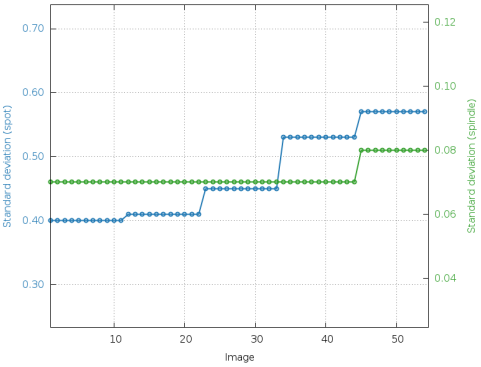

Fig.20 : (sweep m4G4eg) standard deviation (spot position and spindle) as a function of image number

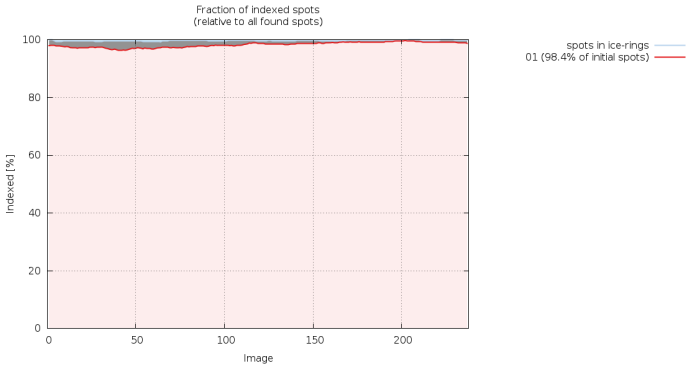

Fig.21 : (sweep m4G4eg-2) number of spots for each indexing solution as a function of image number

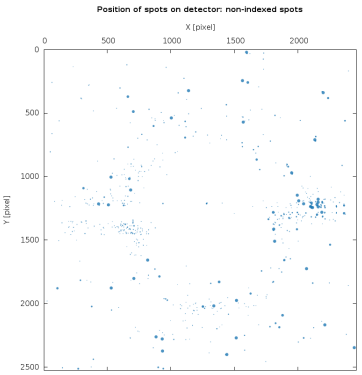

Fig.22 : (sweep m4G4eg-2) unindexed spots as a function of detector position

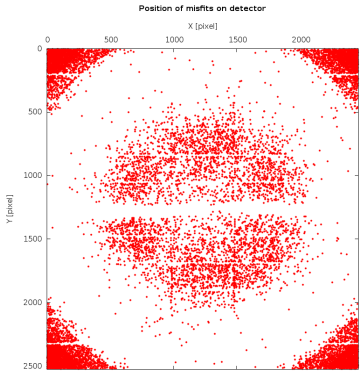

Fig.23 : (sweep m4G4eg-2) reflections classified as misfits (as a function of detector position)

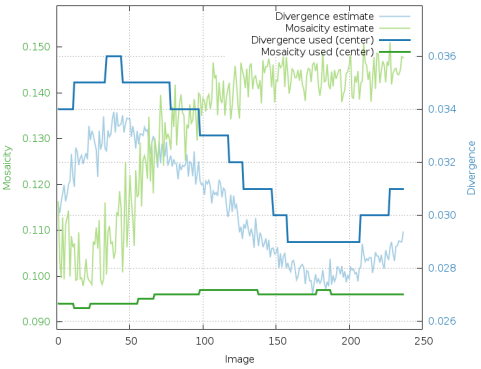

Fig.24 : (sweep m4G4eg-2) divergence and mosaicity (estimated and used) as a function of image number

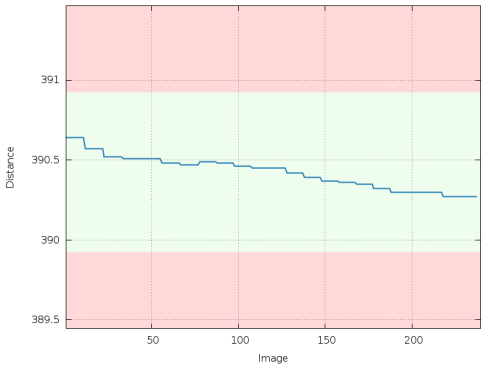

Fig.25 : (sweep m4G4eg-2) refined crystal-to-detector distance as a function of image number

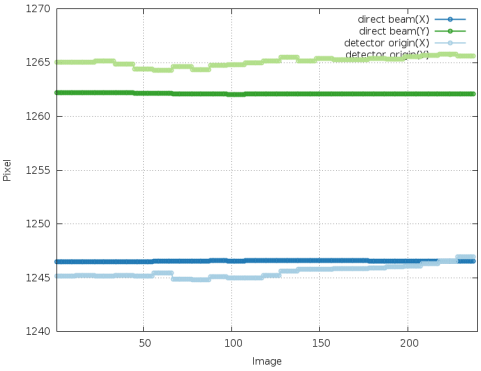

Fig.26 : (sweep m4G4eg-2) direct beam position and detector origin as a function of image number

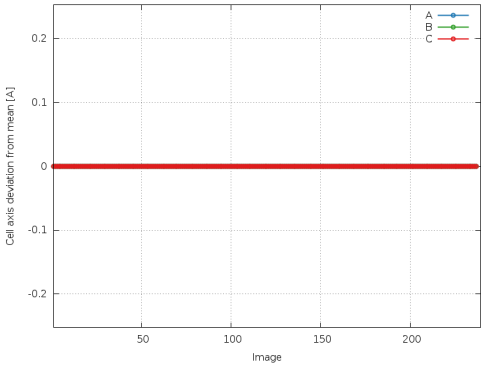

Fig.27 : (sweep m4G4eg-2) deviation of refined cell axes relative to their mean (as a function of image number)

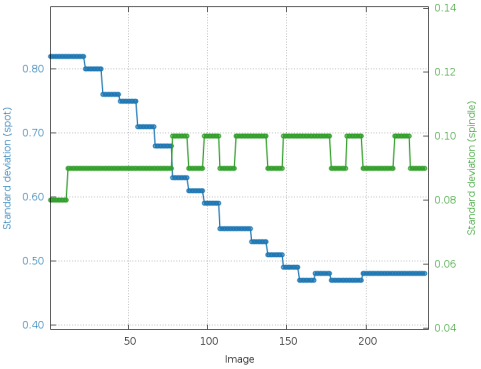

Fig.28 : (sweep m4G4eg-2) standard deviation (spot position and spindle) as a function of image number

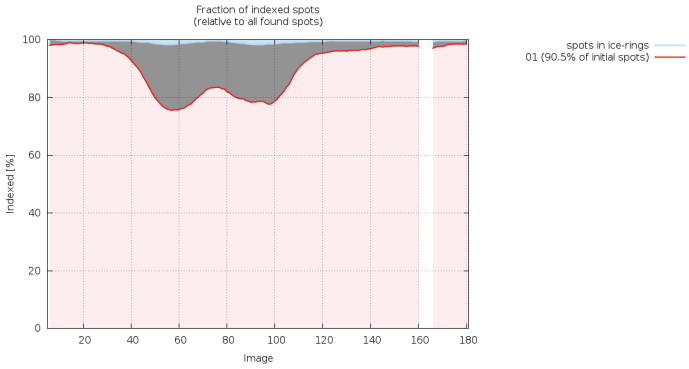

Fig.29 : (sweep m4G4eg-3) number of spots for each indexing solution as a function of image number

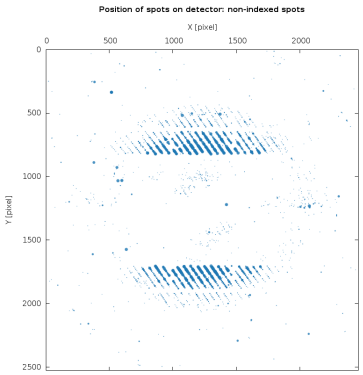

Fig.30 : (sweep m4G4eg-3) unindexed spots as a function of detector position

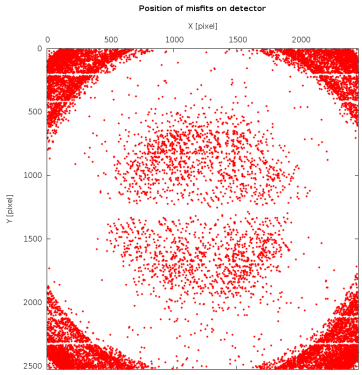

Fig.31 : (sweep m4G4eg-3) reflections classified as misfits (as a function of detector position)

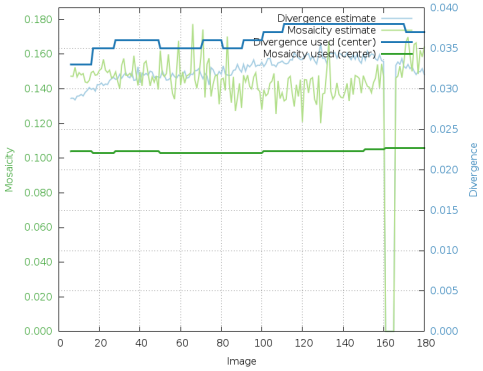

Fig.32 : (sweep m4G4eg-3) divergence and mosaicity (estimated and used) as a function of image number

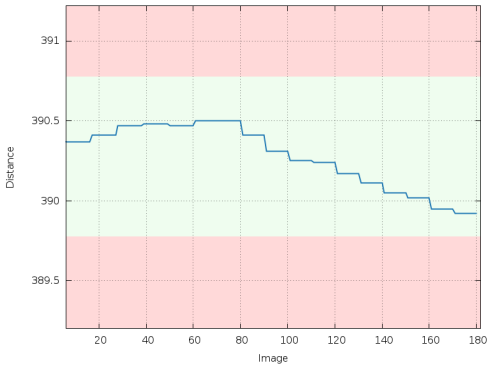

Fig.33 : (sweep m4G4eg-3) refined crystal-to-detector distance as a function of image number

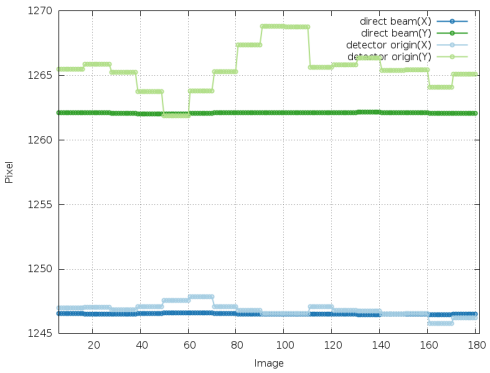

Fig.34 : (sweep m4G4eg-3) direct beam position and detector origin as a function of image number

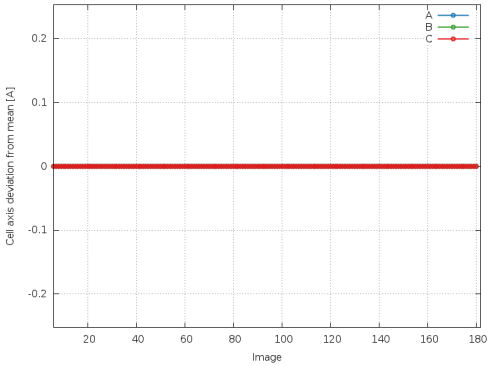

Fig.35 : (sweep m4G4eg-3) deviation of refined cell axes relative to their mean (as a function of image number)

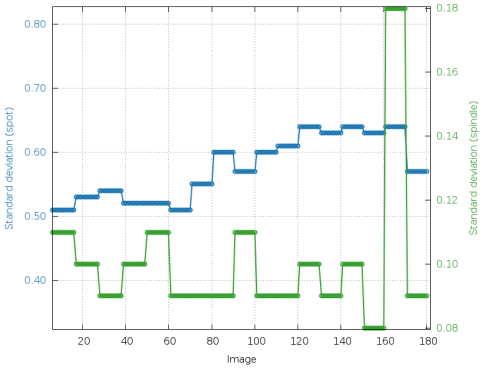

Fig.36 : (sweep m4G4eg-3) standard deviation (spot position and spindle) as a function of image number

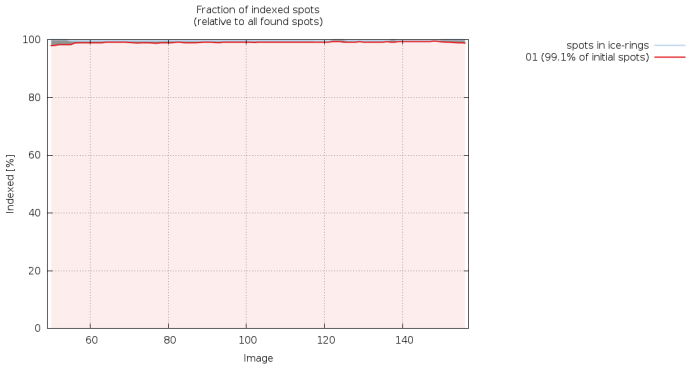

Fig.37 : (sweep m4G4eg-4) number of spots for each indexing solution as a function of image number

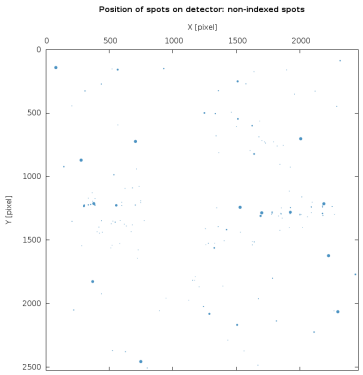

Fig.38 : (sweep m4G4eg-4) unindexed spots as a function of detector position

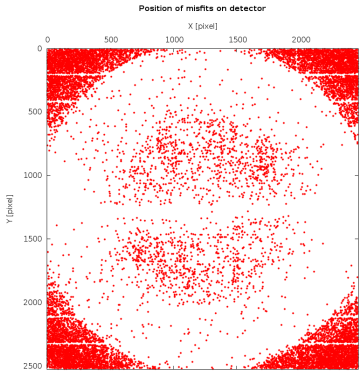

Fig.39 : (sweep m4G4eg-4) reflections classified as misfits (as a function of detector position)

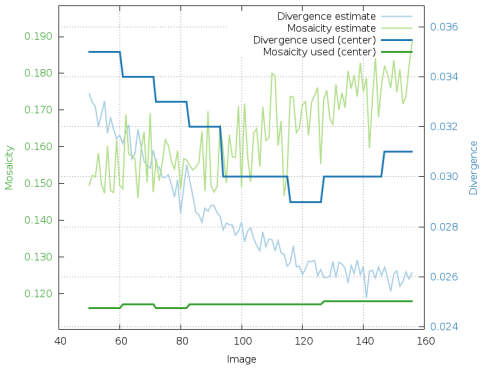

Fig.40 : (sweep m4G4eg-4) divergence and mosaicity (estimated and used) as a function of image number

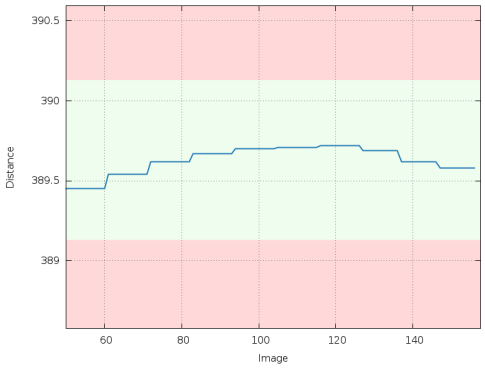

Fig.41 : (sweep m4G4eg-4) refined crystal-to-detector distance as a function of image number

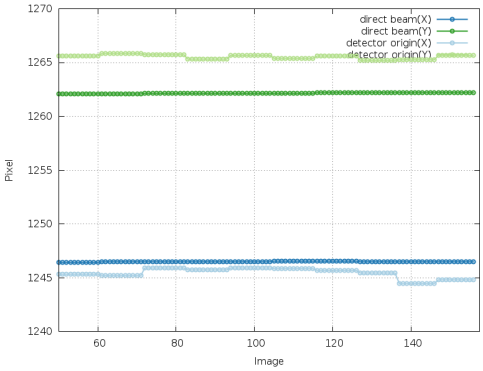

Fig.42 : (sweep m4G4eg-4) direct beam position and detector origin as a function of image number

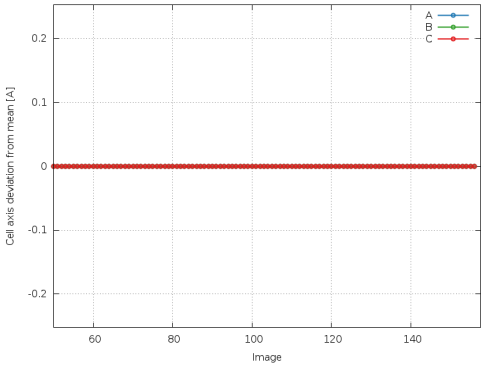

Fig.43 : (sweep m4G4eg-4) deviation of refined cell axes relative to their mean (as a function of image number)

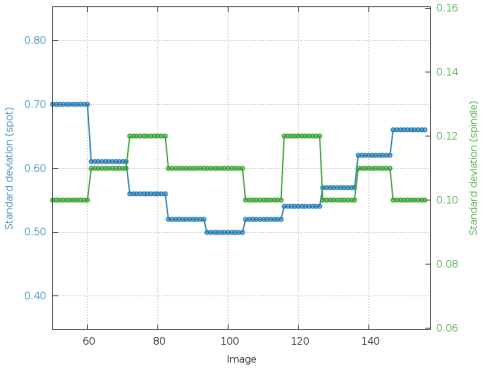

Fig.44 : (sweep m4G4eg-4) standard deviation (spot position and spindle) as a function of image number

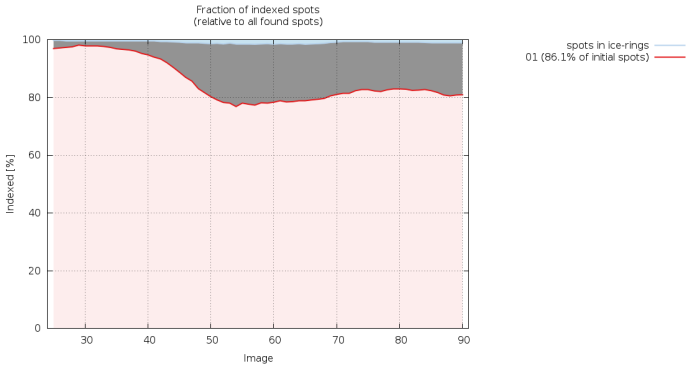

Fig.45 : (sweep m4G4eg-5) number of spots for each indexing solution as a function of image number

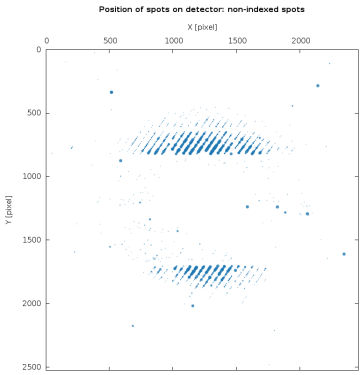

Fig.46 : (sweep m4G4eg-5) unindexed spots as a function of detector position

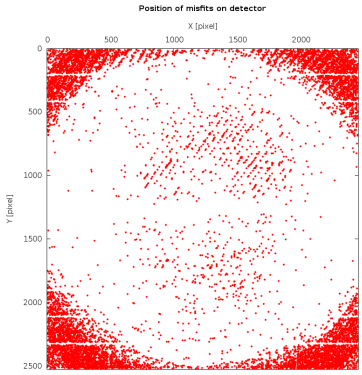

Fig.47 : (sweep m4G4eg-5) reflections classified as misfits (as a function of detector position)

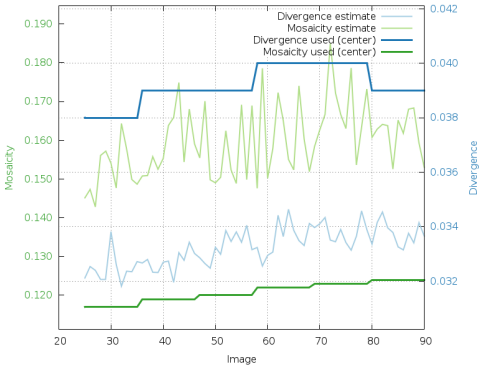

Fig.48 : (sweep m4G4eg-5) divergence and mosaicity (estimated and used) as a function of image number

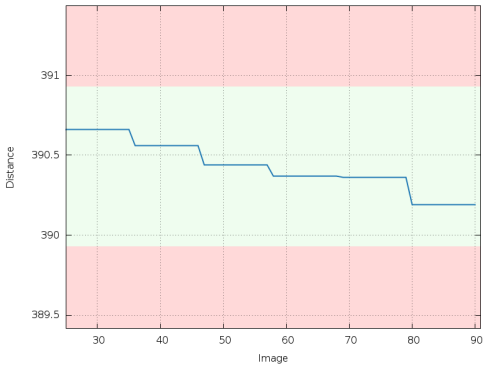

Fig.49 : (sweep m4G4eg-5) refined crystal-to-detector distance as a function of image number

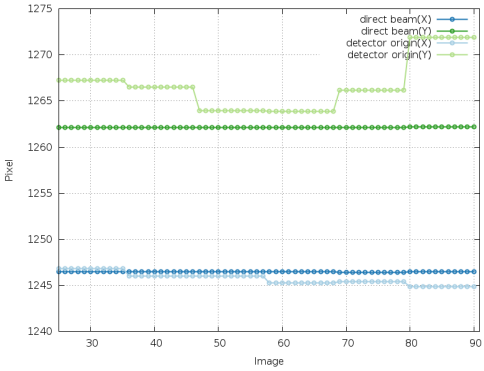

Fig.50 : (sweep m4G4eg-5) direct beam position and detector origin as a function of image number

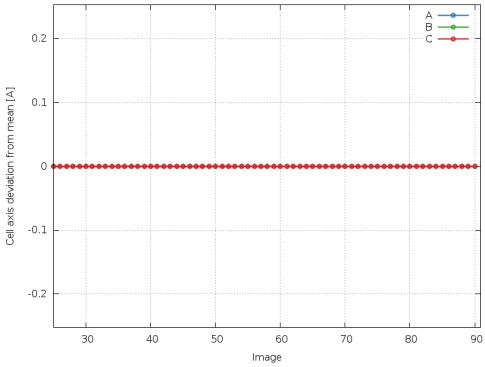

Fig.51 : (sweep m4G4eg-5) deviation of refined cell axes relative to their mean (as a function of image number)

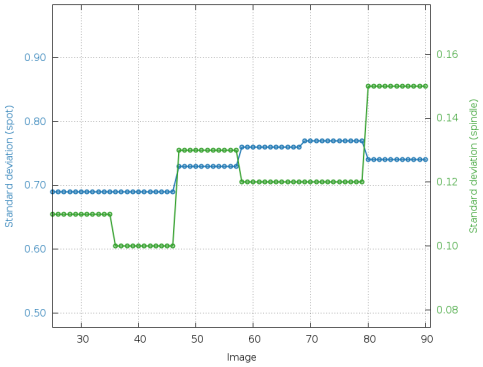

Fig.52 : (sweep m4G4eg-5) standard deviation (spot position and spindle) as a function of image number

autoPROC	Vonrhein, C., Flensburg, C., Keller, P., Sharff, A., Smart, O., Paciorek, W., Womack, T. and Bricogne, G. (2011). Data processing and analysis with the autoPROC toolbox. Acta Cryst. D67, 293-302.
XDS	Kabsch, W. (2010). XDS. Acta Cryst. D66, 125-132.
POINTLESS	Evans, P.R. (2006). Scaling and assessment of data quality, Acta Cryst. D62, 72-82.
AIMLESS	Evans, P.R. and Murshudov, G.N. (2013). How good are my data and what is the resolution?, Acta Cryst. D69, 1204-1214.
CCP4	Winn, M.D., Ballard, C.C., Cowtan, K.D. Dodson, E.J., Emsley, P., Evans, P.R., Keegan, R.M., Krissinel, E.B., Leslie, A.G.W., McCoy, A., McNicholas, S.J., Murshudov, G.N., Pannu, N.S., Potterton, E.A., Powell, H.R., Read, R.J., Vagin, A. and Wilson, K.S. (2011). Overview of the CCP4 suite and current developments, Acta. Cryst. D67, 235-242.
STARANISO	Tickle, I.J., Flensburg, C., Keller, P., Paciorek, W., Sharff, A., Vonrhein, C., and Bricogne, G. (2020). STARANISO. Cambridge, United Kingdom: Global Phasing Ltd.